

Double Relics in Abell 2345 and Abell 1240

spectral index and polarization analysis

A. Bonafede^{1,2}, G. Giovannini^{1,2}, L. Feretti², F. Govoni³, and M. Murgia^{2,3}

¹ Università di Bologna, Dip. di Astronomia, via Ranzani 1, I-40126 Bologna, Italy

² INAF, Istituto di Radioastronomia, via Gobetti 101, I-40129 Bologna, Italy

³ INAF, Osservatorio Astronomico di Cagliari, Strada 54, Loc. Poggio dei Pini, I-09012 Capoterra (Ca), Italy

Received July 14, 2008; accepted September 19, 2008

ABSTRACT

Aims. The aim of the present work is to study the radio properties of double relics in Abell 1240 and Abell 2345 in the framework of double relic formation models.

Methods. We present new Very Large Array observations at 20 and 90 cm for these two clusters. We performed spectral index and polarization analysis and compared our results with expectations from theoretical models.

Results. The presence of double relics in these two cluster is confirmed by these new observations. Double relics in Abell 1240 show radio morphology, spectral index and polarization values in agreement with “outgoing merger shocks” models. One of the relics of Abell 2345, shows a peculiar morphology and spectral index profile, that are difficult to reconcile with present scenarios. We suggest a possible origin for this peculiar relic.

Key words. Galaxies:clusters:general - Galaxies:clusters:individual:A1240, A2345 - Radiation mechanism:non-thermal - Polarization - Magnetic field

1. Introduction

The hierarchical model of structure formation predicts that clusters of galaxies form by subsequent merging of smaller structures. A consistent amount of energy ($\sim 10^{63} - 10^{64}$ ergs) is released in the Intra Cluster Medium (ICM) as result of such merger events. Cosmological numerical simulations have shown that shocks and turbulence associated with these processes do not only heat the ICM but also play an important role in non-thermal phenomena occurring in the ICM (see e. g. the review by Dolag et al. 2008). Although these processes are not completely understood yet, this energy input is supposed to accelerate and inject relativistic particles on cluster scale and amplify the magnetic field in the ICM.

Extended radio sources on cluster scale not associated with any optical counterpart but arising from the ICM have been detected in an increasing number of galaxy clusters. They are called radio halos and radio relics depending on their morphology, location and radio properties.

Radio relics are extended radio sources located at the outskirts of galaxy clusters, and are strongly polarized, with linear fractional polarization at 20 cm above 10 %, reaching values up to 50 % in some regions (see e.g. Govoni & Feretti 2004; Ferrari et al. 2008). Their origin is debated and not well known. There is a general consensus that it is related to phenomena occurring in the ICM during merging events. So far, there are ~ 20 clusters of galaxies where at least one radio relic is present. Their radio morphology and location are quite varied, and could re-

flect different physical origin or ICM conditions (Kempner et al. 2004; Giovannini & Feretti 2004). Due to low X-ray brightness at the cluster periphery, a comparison of relic properties with the surrounding medium (i. e. temperature and brightness gradient induced by shock waves) is not obvious. Feretti & Neumann (2006) did not find any evidence of a temperature jump nearby the Coma cluster relic, and only recently a temperature gradient has been found nearby the relic in Abell 548b by Solovyeva et al. (2008); here a precise orientation of the cluster merger with respect to the line of sight is inferred, and the projected displacement of the relic from the shock is thus explained.

Of particular interest is to explore the connection between merger shock waves and clusters with double relics, i.e. clusters hosting two relic radio sources located in the peripheral region and symmetric with respect to the cluster center. So far a very small number of clusters with two double relics has been found. One of them is Abell 3667 (Röttgering et al. 1997; Johnston-Hollitt et al. 2002). Here the cluster X-ray emission shows an elongated shape, interpreted as the merger axis of two sub-clusters, and relics are displaced symmetrically and perpendicular to the main axis. X-ray, optical and radio properties have been reproduced by a numerical simulation of a merger between clusters with mass ratio of 0.2 by Roettiger et al. (1999). We note however that not all of the predictions made by such simulations could be tested with available data. Apart from Abell 3667, double relics have been observed in Abell 3376 (Bagchi et al. 2006), and interpreted as “Outgoing merger shock waves”. Double relics have also been observed in RXCJ 1314.4-2515 (Feretti et al. 2005; Venturi et al. 2007), but no detailed study on the relics formation has been performed on this cluster so far.

Table 1. VLA observations

Source	RA (J2000)	DEC (J2000)	ν (MHZ)	Bandwidth (MHZ)	Config.	Date	Duration (Hours)
Abell 2345	21 27 12.0	-12 10 30.0	325	3.125	B	16-AUG-2006	2.0
			325	3.125	C	08-DEC-2006	5.4
Abell 1240	11 23 37.0	43 05 15.0	325	3.125	B	05-AUG-2006	2.6
			325	3.125	C	08-DEC-2006	4.7
Abell 2345-1	21 26 43.0	-12 07 50.0	1425	50	C	08-DEC-2006	1.9
Abell 2345-2	21 27 36.0	-12 11 25.0	1425	50	C	08-DEC-2006	2.0
			1425	50	D	09-APR-2007	1.0
Abell 1240-1	11 23 25.0	43 10 30.0	1425	50	C	08-DEC-2006	1.8
			1425	50	D	12-APR-2007	1.0
Abell 1240-2	11 23 50.0	43 00 20.0	1425	50	C	08-DEC-2006	1.9
			1425	50	D	12-APR-2007	1.0
Abell 2345	21 26 57.2	-12 12 49	1490	50	AnB	02-NOV-1991	0.1

Col. 1: Source name; Col. 2, Col. 3: Pointing position (RA, DEC); Col. 4: Observing frequency;

Col 5: Observing bandwidth; Col. 6: VLA configuration; Col. 7: Dates of observation; Col. 8: Net time on source.

Two more candidates for hosting double relics are Abell 2345 (Giovannini et al. 1999) and Abell 1240 (Kempner & Sarazin 2001).

We present here new Very Large Array (VLA) observations of these two clusters at 20 and 90 cm to confirm and study the double relic emission in the framework of relic formation models. Spectral index analysis of both radio relics in the same cluster have not been performed so far. In Abell 3667 the spectral index image has been obtained for only one of the two relics, and no spectral index information are available for relics in Abell 3376. Only integrated spectral index information are available for the relics in RXCJ 1314.4-2515. Study of the spectral index and of the polarization properties of relics offers a powerful tool to investigate the connection between double relics and outgoing shock waves originating in a merger event. In fact, theoretical models and numerical simulations make clear predictions on the relic spectral index trend and magnetic field properties (see Ensslin et al. 1998; Roettiger et al. 1999; Hoeft & Brügger 2007).

The paper is organized as follows: in Sec. 2 observations and data reduction are described, in Sec. 3 and 4 we present the analysis of the cluster Abell 2345 and Abell 1240. Results are discussed in Sec. 5 in comparison with other observed relics and theoretical models, and conclusions are presented in Sec. 6. We assume a Λ CDM cosmological model with $H_0 = 71 \text{ km s}^{-1} \text{ Mpc}^{-1}$, $\Omega_M = 0.27$, $\Omega_\Lambda = 0.73$.

2. VLA radio observations

2.1. Total intensity data reduction

Observations have been performed at the Very Large Array (VLA) at 20 cm in the C and D configuration and at 90 cm in the B and C configuration, in order to obtain the same spatial frequency coverage in the UV plane. Observations details are given in Tab. 1.

Observations at 20 cm (1.4 GHz) have been pointed separately on the two relics in both of the clusters because of the smaller full width at half power of the primary beam. Observations of the cluster Abell 1240 have been calibrated using the source 3C286 as primary flux density calibrator¹. The source 1156+314 has been observed at intervals of about 30 min and used as phase

calibrator. Observations of Abell 2345 have been calibrated using the sources 3C48 as primary flux density calibrator. Phase calibration has been performed by observing the source 2137-207 at intervals of ~ 30 min.

We performed standard calibration and imaging using the NRAO Astronomical Imaging Processing Systems (AIPS). Cycles of phase self-calibration were performed to refine antennas phase solutions, followed by a final amplitude and gain self-calibration cycle.

In addition we recovered from the VLA data archive a short observation performed with AnB array. The source 3C48 is used as primary flux density calibrator and the source 2121+053 is used as phase calibrator. We reduced and calibrated these data as explained above, details are given in Tab. 1.

Observations at 90 cm (325 MHz) have been performed in the spectral line mode, using 32 channels with 3.127 MHz bandwidth. This observing method avoids part of the VLA internal electronics interferences and allows us to remove accurately Radio Frequency Interferences (RFI). This also reduces bandwidth smearing, that is quite strong at low frequencies. Primary flux density and phase calibrators were the same sources used in 1.4 GHz observations. 3C48 and 3C286 were also used for bandpass calibration. RFI are particularly strong at low radio frequency, so that an accurate editing has been done channel by channel, resulting in a consistent flag of data. This in conjunction with bad data coming from EVLA antennas results in a loss of ~ 40 % of observing time. Calibration has been performed following the ‘‘Suggestions for P band data reduction’’ by Owen et al. (2004).

After the initial bandpass calibration channels from 1 to 4 and from 28 to 32 have been flagged because of the roll-off of the bandpass. In the imaging procedure data have been averaged to 8 channels. Imaging has been performed using the wide field imaging technique to correct for non-complanarity effects over a wide field of view. 25 facets covering the main lobe of the primary beam have been used in the cleaning and phase-self calibration processes. We also searched in the NVSS data archive for sources stronger than 0.5 Jy over a radius as large as 10° . These sources have been included in the initial cleaning and self calibration steps.

Each (u,v) data set at the same frequency but observed with different configurations has been calibrated, reduced and imaged separately and then combined to produce the final images. Images resulting from the separate pointed observations

¹ we refer to the flux density scale by Baars & Martin (1990)

at 1.4 GHz have been then linearly combined with the AIPS task LTESS. We combined the data set and produced images at higher and lower resolution (herein after HR images and LR images) giving uniform and natural weight to the data. For the purposes of the spectral analysis, the final images at 325 MHz and 1.4 GHz, have been restored with the same beam (reported in Tab. 2 and 3) and corrected for the primary beam effects.

Table 2. Abell 2345

Source name	ν MHz	θ arcsec	σ_I mJy/beam	Fig.
Abell 2345-1 HR	1425	37 X 20	0.08	
Abell 2345-1 LR	1425	50 X 38	0.09	2, central panel
Abell 2345-2 HR	1425	37 X 20	0.09	
Abell 2345-2 LR	1425	50 X 38	0.09	2, central panel
Abell 2345 HR	325	37 X 20	1.7	
Abell 2345 LR	325	50 X 38	2.0	2, right panels
Abell 2345	1490	6X6	0.13	1, central panel

Col. 1: Source name; Col. 2: Observation frequency;
Col. 3: Restoring beam; Col. 4: RMS noise of the final images;
Col 5: Figure of merit.

Table 3. Abell 1240

Source name	ν MHz	θ arcsec	σ_I mJy/beam	Fig.
Abell 1240-1 HR	1425	22 X 18	0.04	6
Abell 1240-1 LR	1425	42 X 33	0.04	7, central panel
Abell 1240-2 HR	1425	22 X 18	0.04	6
Abell 1240-2 LR	1425	42 X 33	0.05	7, central panel
Abell 1240 HR	325	22 X 18	0.9	
Abell 1240 LR	325	42 X 33	1.0	7, left panels

Col. 1: Source name; Col. 2: Observation frequency;
Col. 3: Restoring beam; Col. 4: RMS noise of the final images;
Col. 5: Fig. of merit.

Table 4. Total and polarization intensity radio images at 1425 MHz

Source name	θ arcsec	σ_I (mJy/beam)	$\sigma_{Q,U}$ (mJy/beam)	Fig.
Abell 2345-1	23 X 16	0.05	0.02	5, right panel
Abell 2345-2	23 X 16	0.07	0.02	5, left panel
Abell 1240-1	18 X 17	0.04	0.02	10, top panel
Abell 1240-2	18 X 17	0.04	0.01	10, bottom panel

Col. 1: Source name; Col. 2: Restoring beam;
Col. 4: RMS noise of the I image; Col 5: RMS noise of the Q and U images
Col 6: Figure of merit.

2.2. Polarization intensity data reduction

Observations at 20 cm (1.425 GHz) include full polarization information. Polarization data observed with the D array are unusable because of bad quality of data of the polarization calibrator. The absolute polarization position angle has been calibrated by observing 3C286 for both clusters in C configuration. The instrumental polarization of the antennas has been corrected using the source 1156+314 for Abell 1240 and the

source 2137-207 for Abell 2345.

Stokes parameters U and Q images have been obtained. We then derived the Polarization intensity image ($P = \sqrt{U^2 + Q^2}$), the Polarization angle image ($\Psi = \frac{1}{2} \arctan \frac{U}{Q}$) and the Fractional Polarization image ($FPOL = \frac{P}{I}$), with I being the total intensity image. Further details are given in Tab. 4.

3. The Cluster Abell 2345

Optical information are available for this cluster, while little is known about its X-ray emission. General data are reported in Tab. 5.

Weak gravitational lensing analysis has been performed by Dahle et al. (2002) and by Cypriano et al. (2004). Optical data cover the inner part of the cluster ($\sim 3' \times 3'$). They find that this cluster has a well defined core dominated by a cD galaxy, and both the light and galaxy number density distribution have several peaks close to the central galaxy. The authors derived that the projected mass distribution has the most prominent peak displaced from the central cD by $\sim 1.5'$, although a secondary peak is closer to the central cD. No information about the possible presence of a cooling flow associated with this galaxy is present in the literature. Dahle et al. (2002) conclude from their analysis that the cluster may be a dynamically young system. Cypriano et al. (2004) report the mass distribution derived from weak lensing analysis and find that the best fit to their data is a singular isothermal ellipsoid with the main axis oriented in the E-W direction.

The radio emission of Abell 2345 is characterized by the presence of two relics visible in the NVSS (Giovannini et al. 1999).

Our new VLA observations confirm the presence of two regions where non-thermal emission is present at the cluster periphery, nearly symmetrical with respect to the cluster center. These new observations together with the archive data, allow the study of the cluster radio emission in a wide range of resolutions going from $\sim 6''$ to $\sim 50''$. Therefore, it is possible to separate the contribution of discrete sources whose emission is not related to the relic's physical properties. In Fig. 1 the radio emission of Abell 2345 at $6''$ resolution is shown overlaid onto the optical emission (taken from the Digitalized Palomar Sky Survey II, red band). Two central radio-tail sources are associated with optical galaxies in the cluster center. The central cD is visible in the optical image. Relics are not visible in this image because of the lack of short baselines. This confirms that the emission detected in lower resolution observations is indeed extended and it is not due to the blending of discrete sources. In the same figure we also report the radio relic emission as detected by C array observations. The western relic (Abell 2345-1) is located at ~ 1 Mpc from the cluster X-ray center while the eastern relic (Abell 2345-2) is ~ 890 kpc far from the cluster center (see Tab. 6).

There are several discrete sources in proximity of the western relic, A2345-1, visible in the 1.4 GHz image, they are labeled with letters from A to F in the right panel of Fig.1. The sources A, C, D, E and F could be associated with the optical galaxies visible in the DPOSSII image, whereas B does not have any obvious optical identification. Optical emission is present at $35''$ in NE direction from the radio peak. This is larger than the error associated with the beam, that is only $6'' \times 6''$ in the highest resolution image. We can then conclude that no optical counterpart of the B radio source is detected in the DPOSSII

Table 5. Abell 2345 and Abell 1240 properties

Source name	RA (J2000)	DEC (J2000)	z	scale (kpc/'')	F_X 10^{-12} erg/s/cm 2	L_X 10^{44} erg/s
Abell 2345	21 27 11.00	-12 09 33.0	0.1765	2.957	5.3	4.3
Abell 1240	11 23 32.10	43 06 32	0.1590	2.715	1.3	1.0

Col. 1: Source name; Col. 2, Col. 3: Cluster X-ray centre (RA, DEC); Col 4: Cluster redshift; Col 5: arcsec to kpc conversion scale;

Col 6: Flux in the 0.1- 2.4 keV band (Abell 2345) and in the 0.5-2 keV (Abell 1249); Col 7: X-ray cluster luminosity in the 0.1-2.4 keV band (Abell 2345) and in the 0.5-2 keV (Abell 1240);

Data from Böhringer et al. (2004) for Abell 2345 and from David et al. (1999) for Abell 1240, corrected for the adopted cosmology.

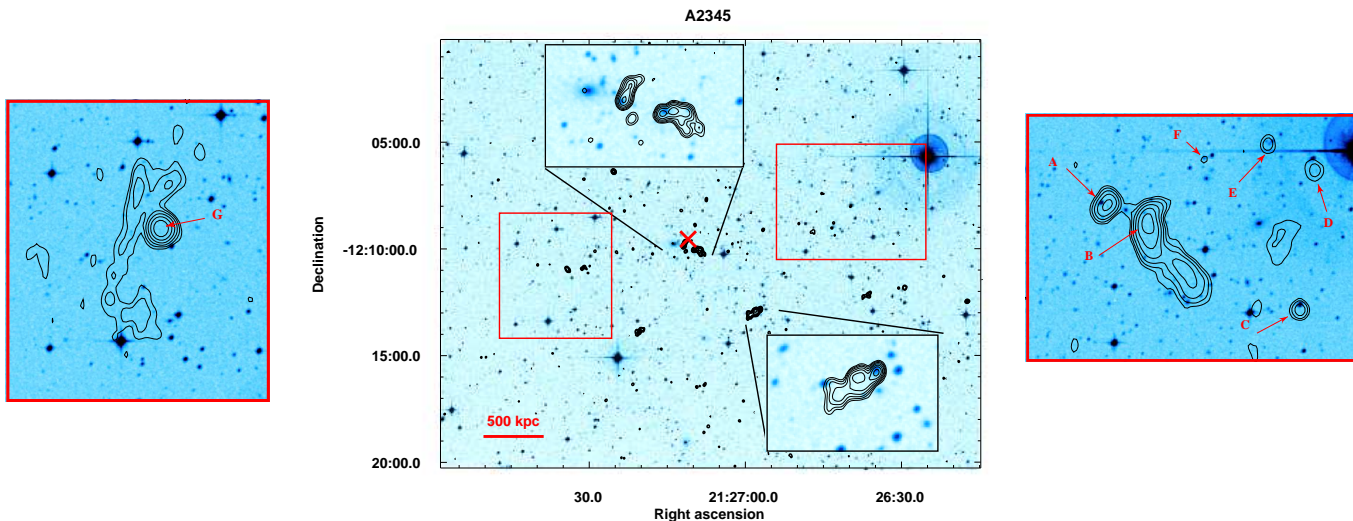


Fig. 1. The cluster Abell 2345. In the center: DPOSSII optical emission (red band) in colors overlaid onto radio contours at 1.490 GHz. First contours are ± 0.4 mJy/beam and are then spaced by a factor 2. The beam in $6'' \times 6''$. Top inset shows the zoomed images of the central sources: the central cD galaxy and two radio galaxies are visible. Bottom inset shows the zoomed image of the southern radio source. Red Boxes mark the region of the relics, completely resolved in the high resolution image. In the Left and Right panels zoomed image of the red boxes is shown. Here colors represent the optical DPOSSII emission, while contours represents the relic radio emission at the resolution of $23'' \times 16''$. The relic A2345-1 is visible in the right panel, while A2345-2 is in the left panel. Contours start at ± 0.15 mJy/beam and are spaced by a factor 2. Red arrows indicate the position of the discrete sources embedded in the relic emission.

image. The sources D E and F are not visible in the 325 MHz image (see Fig. 2, top left panel). This is consistent with a radio source having a spectral index $< 1.2^2$. There is only one discrete source in proximity of the relic A2345-2, labeled with G in the Fig.1 without any obvious optical identification. This source is also detected in the higher resolution image.

The whole extension of the relics is properly revealed by LR images (Fig. 2). The morphology of the relics is similar at 1.4 GHz and 325 MHz, although only the brightest regions can be seen at 325 MHz due to the higher rms noise level of these observations with respect to the 1.4 GHz ones. The total flux of the relics at the 2 frequencies, excluding the contribution of the discrete sources, are reported in Tab. 6, where the main physical parameters are summarized.

The relic A2345-1 shows an elongated shape at high resolution, while at lower resolution it shows a weaker wide emission extending in the West direction i.e. toward the cluster outskirts. We note that this circular filamentary morphology is not seen in other double relic sources, as discussed in the introduction.

3.1. Spectral index analysis

We derived the spectral index image of the cluster's relics comparing the LR images at 1.4 GHz and 325 MHz. The rms noise of the images are reported in Tab. 2. Spectral index and spectral index noise images are shown in Fig. 2. They have been obtained by considering only pixels whose brightness is $> 3\sigma$ at both frequencies. We note that relics are more extended at 1.4 GHz than at 325 MHz. This can be due to the different sensitivities at 1.4 GHz and 325 MHz. Confusion and RFI strongly affect the low frequency image, where the noise level is significantly higher than the thermal noise. A consistent spectral index analysis has to consider the different extension at the two frequencies. In fact, as already pointed out by Orrú et al. (2007) if we compute spectral index analysis considering only regions that have a signal to noise ratio > 3 at both frequencies, we introduce a bias, since we are excluding a priori low spectral index regions, whose emission cannot be detected at 325 MHz. For instance, the relic A2345-1 radio brightness at 1.4 GHz decreases as the distance from the cluster center increases. The fainter region could be detected in the 325 MHz image only if its spectral index, α , were steeper than ~ 1.8 .

In both of the relics the spectral index is patchy. The spectral index rms is $\sigma_{spi} \sim 0.4$ while the mean spectral index noise is

² The spectral index α is derived according to $S_\nu \propto \nu^{-\alpha}$.

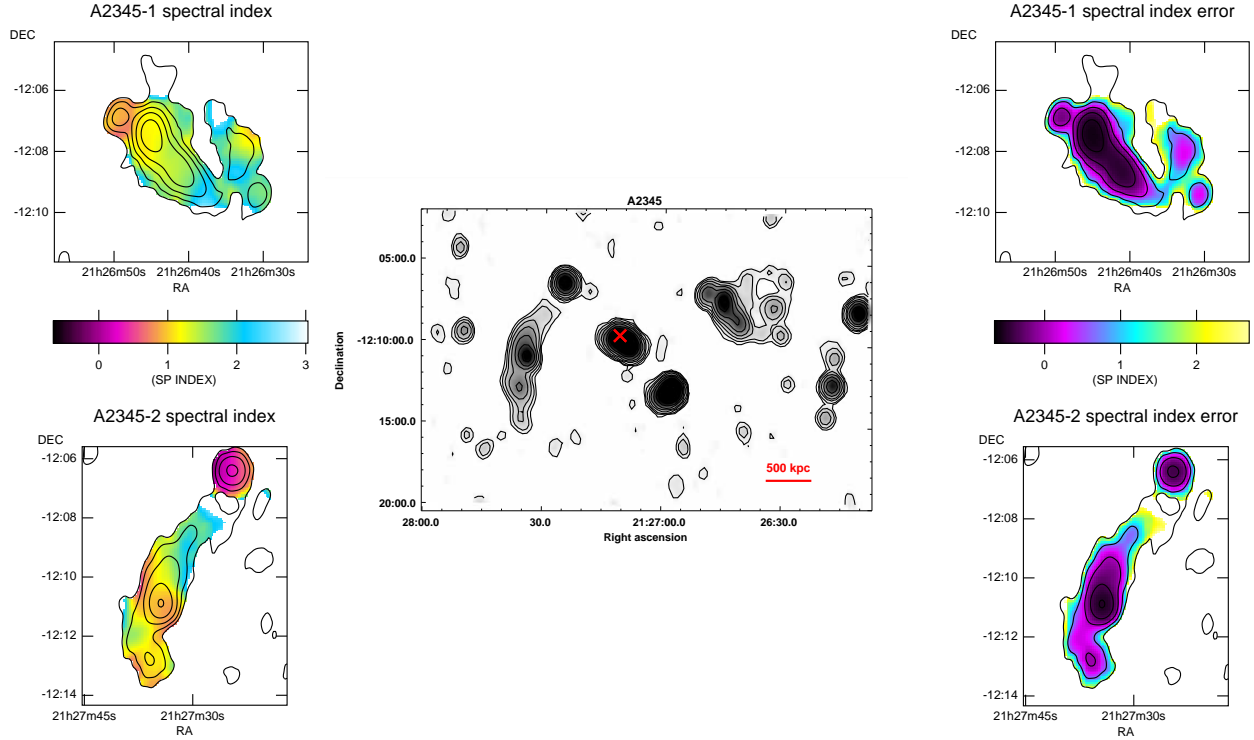


Fig. 2. Center: the cluster Abell 2345 radio emission at 1.4 GHz. The beam is $50'' \times 38''$. Contours start at 3σ (0.24 mJy/beam) and are then spaced by a factor 2. The cross marks the X-ray cluster center. Left: Colors represent the spectral index of the relic A2345-1 (top) and A2345-2 (bottom) superimposed over the radio emission at 325 MHz (contours). The beam is $50'' \times 38''$, contours start at 3σ (6 mJy/beam) and are then spaced by a factor 2. Right: Spectral index error image (colors) superimposed onto the emission at 325 MHz (contours are as above).

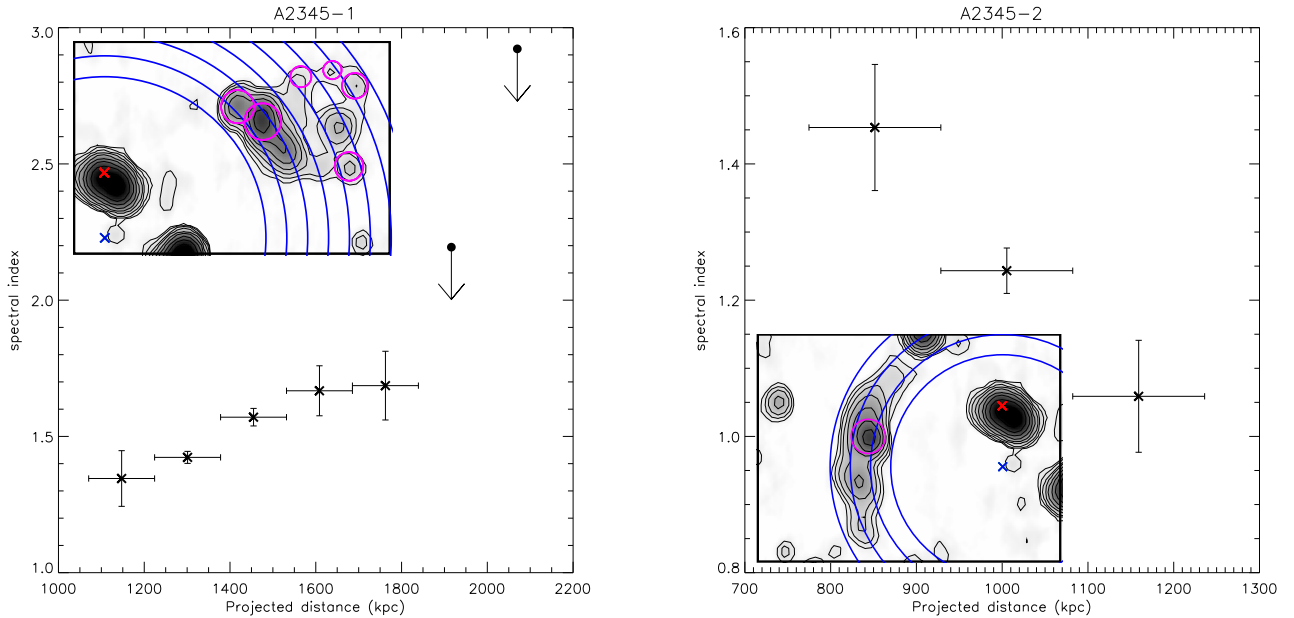


Fig. 3. Spectral index radial trend of A2345-1 (left) and A2345-2 (right), computed in shells of $\sim 50''$ in width. It has been computed excluding the contribution of the discrete sources. Crosses refer to spectral index values computed in shells where the mean brightness is $> 3\sigma$ at both 325 MHz and 1.4 GHz. Arrows are 3σ upper limits on the spectral index mean value (see text). The red cross refers to the cluster X-ray center, the blue cross refers to the center of the spherical shells. In the insets: displacement of the shells over which the mean spectral index has been computed. Circles refer to the discrete sources embedded in the relic emission. The red cross refers to the cluster X-ray center, the blue cross is the center of the spherical shells.

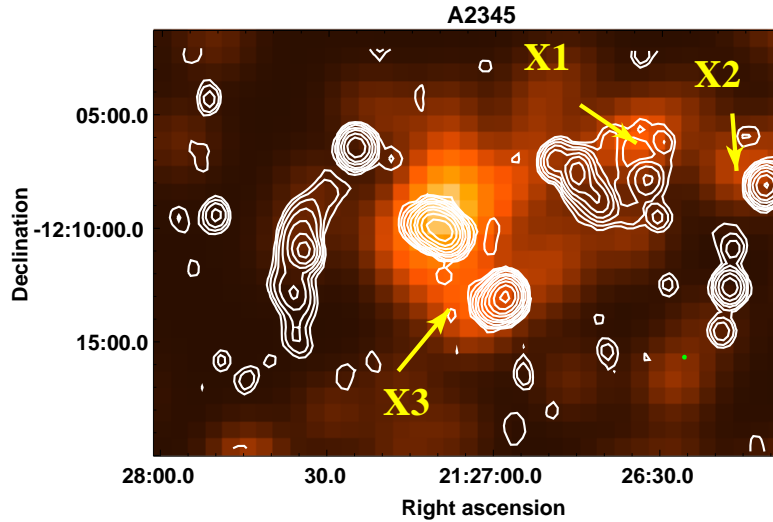


Fig. 4. Abell 2345 X-ray emission (colors) in the energy band 0.1-2.4 keV from ROSAT PSPC observations. The image has been smoothed with a Gaussian of $\sigma \sim 60''$; contours represent the radio image of the cluster at 1.4 GHz. The beam is $50'' \times 38''$. Contours are 0.24 mJy/beam and are then spaced by a factor 2. Arrows mark the position of the X1 X2 and X3 regions.

$\langle \text{Spix Noise} \rangle \sim 0.1$ for both relics. Thus, by comparing these two quantities we can conclude that spectral index features are statistically significant.

Our aim here is to investigate if there is a systematic variation of the relic spectral index with distance from the cluster center as found in other radio relics (e.g. 1253+275 by Giovannini et al. 1991; Abell 3667 by Röttgering et al. 1997; Abell 2744 by Orrú et al. 2007; Abell 2255 by Pizzo et al. 2008; Abell 521 by Giacintucci et al. 2008;).

In order to properly obtain the radial trend of the spectral index, we integrated the radio brightness at 325 MHz and 1.4 GHz in radial shells of $\sim 50''$ in width wherever the 1.4 GHz brightness is $> 3\sigma$, and then we computed the value of the spectral index in each shell. We have excluded the regions where discrete radio sources are embedded in the relic emission (see insets in Fig. 3). The shells have been centered in the extrapolated curvature center of the relic A2345-2, that is $2.6'$ South the cluster X-ray center. Shells are then parallel to the relics main axis. We computed the integrated brightness in each shell at 20 and 90 cm, and calculated the associated error as $\sigma \times \sqrt{N_{beam}}$, where σ is the image rms noise, N_{beam} is the number of beams sampled in the shell. In those shells where the brightness is $> 3\sigma$ in the 1.4 GHz image but $< 3\sigma$ in the 325 MHz image, only upper limits on the mean spectral index can be derived. The spectral index profiles thus obtained are shown in Fig. 3. These plots shows that the spectral index in the relic A2345-1 increases with distance from the cluster center, indicating a spectral steepening of the emitting particles. The spectral index, in each shell, is rather high, going from ~ 1.4 in the inner rim to ~ 1.7 in the central rim of the relic. The spectral index trend derived for the outer shells is consistent with a further steepening.

The spectral index of the relic A2345-2 shows instead a different trend, going from ~ 1.4 in the inner shell to ~ 1.1 in the outer rim (Fig. 3).

3.2. Radio-X-ray comparison

No X-ray studies are present in the literature for this cluster. X-ray observations in the energy band 0.1 – 2.4 keV have been retrieved by the ROSAT data archive. The cluster is $\sim 100'$ offset from the ROSAT pointing. Observations have been performed with the ROSAT PSPC detector for a total exposure time of ~ 14 ksec. After background subtraction the event file has been divided by the exposure map. We smoothed the resulting image with a Gaussian of $\sigma = 60''$. The resulting image is shown in Fig. 4.

The X-ray emission of this cluster is elongated in the NW-SE direction. Two bright regions are visible at $\sim 10'$ and $14'$ in N-W direction from the cluster center (we refer to them as X1 and X2 respectively). The galaxy J21263466-1207214 (RA = 21h26m34.6s, DEC = -12d07m22s, $z=0.178221$) is close to the first one. Another bright region is present at $\sim 4'$ South from the cluster center (X3).

Data presented here allow an interesting comparison among cluster emission at different wavelengths. We note that mass distribution from weak lensing studies (Cypriano et al. 2004) is well represented by an ellipsoid with the major axis directed in the E-W direction and relics are found perpendicular to this axis. Consistently with the optical analysis, the X-ray emission is elongated in the NW-SE direction, indicating a possible merger along that direction, and relics are displaced perpendicular to that axis. In Fig. 4 the X-ray emission is superimposed onto radio contours. A2345-2 is located at the edge of the X-ray emission, as found in relics of Abell 3667 and A3376. A2345-1, instead, is located between eastern edge of the cluster and the X1 region, $10'$ from Abell 2345 center, and its radio emission extends toward X1.

From the same figure, in the X3 region a Narrow Angle Tail radio galaxy is visible in radio images at every resolution (see Fig.1 and 2). Although redshift is not available for this radio source, its structure favors a connection to the cluster and/or to the close X-ray peak. One possibility is that these X-ray multiple features are galaxy clumps interacting with Abell 2345. A self consistent scenario arises from this analysis, indicating

that the cluster Abell 2345 could be undergoing multiple merger with X3 and X1 groups, and this could explain the peculiar properties of A2345-1. More sensitive and resolved X-ray observations in conjunction with optical studies are required to shed light on the connection between the radio emission of A2345, X1 X2 and X3.

3.3. Equipartition Magnetic field

Under the assumption that a radio source is in a minimum energy conditions, it is possible to derive an average estimate of the magnetic field strength in the emitting volume (see e.g. Pacholczyk 1970). We assume that the magnetic field and relativistic particles fill the whole volume of the relics, and that energy content in protons and electrons is equal. We further assume that the volume of the relics is well represented by an ellipsoid having the major and minor axis equal to the largest and smallest linear scale visible in our images; we estimated the third axis to be the mean between the major and minor one. The synchrotron luminosity is calculated from a low frequency cut-off of 10 MHz to a high frequency cut-off of 10 GHz. The emitting particle energy distribution is assumed to be a power law in this frequency range ($N(E) \propto E^{-p}$), with $p = 2\alpha + 1$. We used the mean value of $\alpha = 1.5$ and 1.3 for A2345-1 and A2345-2 respectively and found $B_{eq} \sim 1.0 \mu\text{G}$ in A2345-1 and $0.8 \mu\text{G}$ in A2345-2. These values are consistent with equipartition magnetic field found in other relics.

It has been pointed out by Brunetti et al. (1997) that synchrotron luminosity should be calculated in a fixed range of electron energies rather than in a fixed range of radio frequencies (see also Beck & Krause 2005). In fact, electron energy corresponding to a fixed frequency depends on the magnetic field value, and thus the integration limits are variable in terms of the energy of the radiating particles. Given the power law of the radiating particles and the high value of the radio spectral index, the lower limit is particularly relevant here. We adopted a low-energy cut off of $\gamma_{min}=100$ and assumed $\gamma_{max} \gg \gamma_{min}$, obtaining $B'_{eq} \sim 2.9 \mu\text{G}$ in A2345-1 and $2.2 \mu\text{G}$ in A2345-2.

We derived the minimum non thermal energy density in the relic sources from B'_{eq} obtaining $U_{min} \sim 8.1$ and $4.3 \cdot 10^{-13} \text{erg/cm}^{-3}$ for A2345-1 and A2345-2. The corresponding minimum non-thermal pressure is then ~ 5.0 and $2.7 \cdot 10^{-13} \text{erg/cm}^{-3}$.

We are aware that the extrapolation to low energies or frequencies could over estimate the number of low energy electrons, leading to over estimate the equipartition magnetic field if a spectral curvature is present. We note that a detailed study of the radio spectrum on a large frequency range is available for three peripheral relics: the one in Abell 786, in the Coma cluster (see Giovannini & Feretti, 2004 and references therein) and in Abell 521 (Giacintucci et al. 2008). In these relics a straight steep radio spectrum is observed. We also note that a low frequency cut-off of 10 MHz and a magnetic field of $\sim 1 \mu\text{G}$ imply a low energy cut-off of $\gamma_{min} \sim 1500$. Thus, also if the spectrum of the emitting particles is truncated at $\gamma > 1500$, both B'_{eq} and B_{eq} could over estimate the magnetic field strength. Future low-frequency radio interferometers such as SKA and LWA will likely shed light on this point. On the other hand, it is possible to derive an independent estimate of the magnetic field from X-ray flux due to inverse Compton scattering of CMB photons by relativistic electrons in the relic source. These studies have been performed so far on a scarce number of radio relics and have led to lower limits on the magnetic field strength: $B > 0.8 \mu\text{G}$ in the relic 1140+203 of Abell 1367 (Henriksen & Mushotzky

2001); $B > 1.05 \mu\text{G}$ in 1253+275 of the Coma cluster (Feretti & Neumann 2006; $B > 0.8 \mu\text{G}$ in 0917+75 in Rood27 cluster (Chen et al. 2008); and $B > 2.2 \mu\text{G}$ in the relic 1401-33 in the Abell S753 cluster (Chen et al. 2008). In these cases, the lower limits derived from IC arguments are consistent with equipartition estimates, thus indicating that the equipartition value could be used as a reasonable approximations of the magnetic field strength in relics.

3.4. Polarization analysis

Another important set of information about the magnetic field in the relics can be derived through the study of polarized emission. As previously mentioned, we could calibrate polarization only for observations at 1.4 GHz with the C array.

In Fig. 5 the P radio image of the cluster is shown. The noise achieved in the P, Q and U images (Tab. 4) are lower than those obtained in total intensity image. In fact total intensity image are affected by dynamical range limitation due to the presence of powerful radio sources near our target. These sources are not strongly polarized, so that P images are not affected by such limitation, and weaker polarized emission can be revealed. We note in fact that polarized radio emission of the relic A2345-2 reveals an arc-like structure that is more extended than in total intensity emission. The arc-like structure of this relic indicates that the shock wave, possibly responsible of the radio emission, has been originated $\sim 2.6'$ southern the present X-ray center.

The mean fractional polarization is $\sim 22\%$ in A2345-2, reaching values up to 50% in the eastern region. The relic A2345-1, shows a mean fractional polarization of $\sim 14\%$ with higher polarized region ($\sim 60\%$) in the north-western part of the relic. The amount of fractional polarization allows to estimate the level of order of the magnetic field in the source. Following Burn (1966), if we assume that the magnetic field is composed by an ordered component \mathbf{B}_o plus a random isotropic component represented by a Gaussian with variance equal to $2/3B_r^2$, it results

$$P_{oss} = P_{intr} \frac{1}{1 + (B_r^2/B_o^2)} \quad (1)$$

where P_{oss} is the observed fractional polarization, while P_{intr} is given by $P_{intr} = \frac{3\delta+3}{3\delta+7}$. For the relic A2345-1 we obtain that $B_r^2/B_o^2 \sim 4$, meaning that the magnetic energy density in the random component is three times larger than the one in the ordered component. For the relic A2345-2, instead, we obtain that $B_r^2/B_o^2 \sim 2$. This indicates that the magnetic field in the region of the relic A2345-2 has a higher degree of order. We also have to consider possible beam depolarization, internal depolarization and ICM depolarization, so that what we can conclude from this analysis is $B_r^2/B_o^2 < 4$ and < 2 in A2345-1 and A2345-2 respectively.

In A2345-1 the magnetic field is mainly aligned with the sharp edge of the radio emission, i.e. in the SW-NE direction. In the northern part of the relic the E vectors rotate and in the N-W part they are almost aligned toward the SW-NE direction. In A2345-2 the E vectors are perpendicular to the relic major axis, following the arc-like structure that is marginally visible in the total intensity image.

3.5. Results on Abell 2345

The presented analysis confirms that non-thermal emission is associated with the ICM of Abell 2345.

Table 6. Abell 2345

Source name	Proj. dist kpc	LLS kpc	F_{20cm} mJy	F_{90cm} mJy	$B_{eq} - B'_{eq}$ μG	$\langle \alpha \rangle$
Abell 2345-1	$340''=1000$	$390''=1150$	30.0 ± 0.5	291 ± 4	1.0 -2.9	1.5 ± 0.1
Abell 2345-2	$300''=890$	$510''=1500$	29.0 ± 0.4	188 ± 3	0.8 -2.2	1.3 ± 0.1

Col. 1: Source name; Col. 2: projected distance from the X-ray centroid; Col. 3: Largest linear scale measured on the 20 cm images.
Col. 4 and 5: Flux density at 20 and 90 cm; Col. 6: equipartition magnetic field computed at fixed frequency - fixed energy
(see Sec. 3.3); Col. 7: mean spectral index in region where both 20 and 90 cm surface brightness is $> 3\sigma$

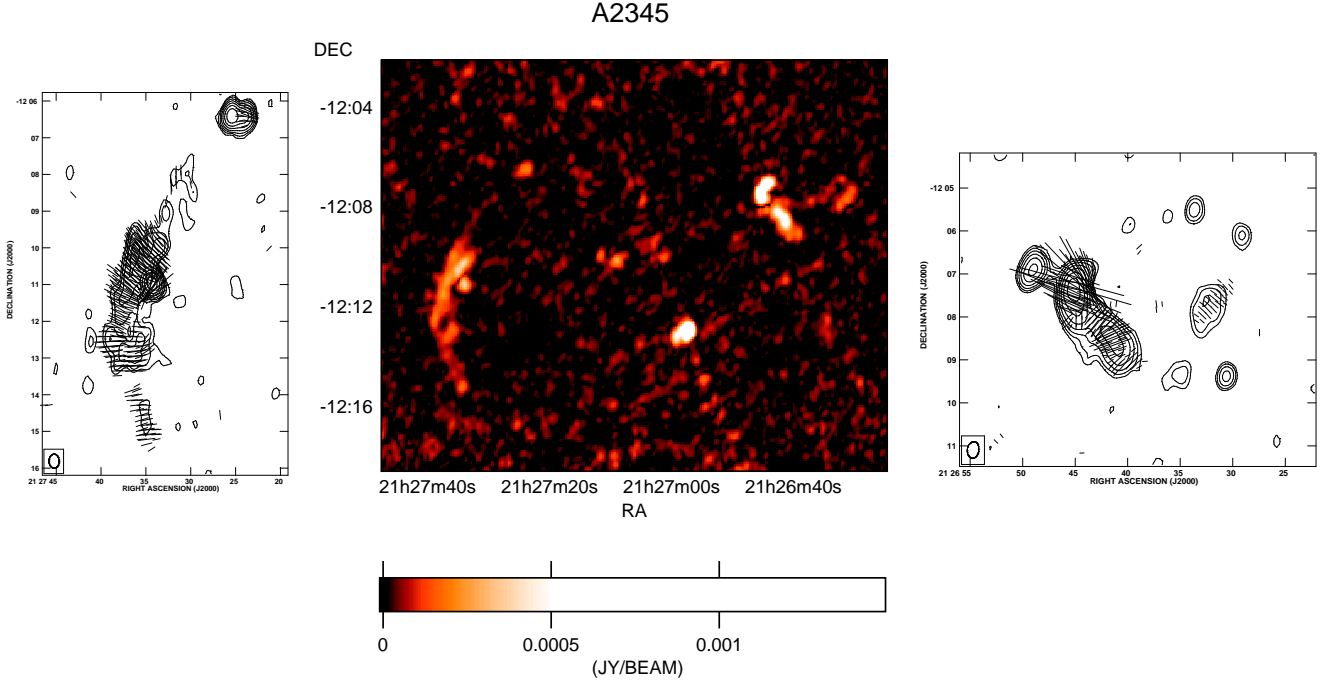


Fig. 5. Abell 2345: Polarized emission of Abell 2345 at 1,4 GHz. In the central panel the polarized radio emission at 1.4 GHz is shown. The restoring beam is $23'' \times 16''$. Left and right panels: contours refer to the radio image Abell 2345-2 and Abell 2345-1 (see Tab. 4 for further details). Contours start from 3σ and are spaced by a factor 2. E vectors are superimposed: line orientation indicates the direction of the E field, while line length is proportional to the polarization intensity (Left panel: $1''$ corresponds to $5.5 \mu\text{Jy}/\text{beam}$; Right panel: $1''$ corresponds to $10 \mu\text{Jy}/\text{beam}$)

- The properties of the western relic, A2345-1 are quite peculiar. We note indeed that its morphology is rather circular and filamentary, its brightness distribution is higher in the inner region of the relic and its spectral index steepens toward the cluster periphery. Although the statistic is really poor, these features have not been found in other double relics so far. The level of polarization, the magnetic field direction mainly aligned with the sharp edge of the radio emission, and the value of the equipartition magnetic field are instead in agreement with other observed relics.

Diffusive shock acceleration models predict a steepening of the radio spectrum towards the cluster center (e.g. Ensslin et al. 1998; Hoeft & Brüggén 2007) as a consequence of the electron energy losses after shock acceleration. It is worth mentioning here that theoretical predictions rely on some assumptions about the shock symmetry and the magnetic field structure that could be not representative of this specific cluster environment. Moreover, if the relic is not seen edge on, projection effects could further complicate the observed radio emission. Taking all of these into account, the observed spectral index trend of A2345-1 cannot be used as an argument to exclude an outgoing shock wave.

We however note that the position of A2345-1 is in between the main cluster and the possibly merging group X1. Thus we suggest the possibility that its radio properties could be affected by this ongoing merger. In particular, if the relic is seen edge-on, and if the magnetic field strength is almost uniform in the relic region, the observed spectral index trend could be the sign of a shock wave moving inward, toward the cluster center. It could result from the interaction with X1. Detailed optical and X-ray observations would be needed to shed light on this point.

- The relic A2345-2 shows the classical feature of “elongated relic sources” also found in double relics of Abell 3667 and Abell 3376, as well as in single relic sources as 1253+275 (Andernach et al. 1984, Giovannini et al. 1991) and A521 (Ferrari 2003, Giacintucci et al. 2008). It is located far from the cluster center, its spectral index is steep with mean value ~ 1.3 and steepens towards the cluster center, as expected by relic formation theories if the relic is observed edge-on. The value of the equipartition magnetic field, the direction of the E vectors and the detected level of polarization are consistent with previous observations of elongated relics

and agree with expectations from theoretical models as well. The polarized emission image reveals the arc-like structure of the relic A2345-2. If we assume that the relic is originated by a spherical shock wave, we can infer the propagation center of the shock by extrapolating the curvature radius of the relic. It results that the propagation center is $\sim 2.6'$, southern the present X-ray center of the cluster Abell 2345 (see Fig. 3).

This corresponds to a physical distance of 450 kpc at this redshift. From weak lensing analysis the galaxy velocity dispersion in this cluster results ~ 900 km/s (Dahle et al. 2002; Cypriano et al. 2004). As we will see in Sect.5, the expected Mach number is of about 2.2 for this relic. Since the galaxy velocity dispersion is comparable to the sound speed in the ICM (see e.g. Sarazin 1988), a Mach number 2.2 corresponds to a velocity of ~ 2000 km/s. The relic A2345-2 is ~ 800 kpc far from the spherical-shock center. A shock wave with $M \sim 2.2$ travels this distance in ~ 0.4 Gyr (if the shock speed remains constant). Thus the merging between the two substructures should have occurred at ~ 1200 km/s to explain the shift of the X-ray center in this scenario. This is a reasonable value for cluster merger velocity.

Although a precise estimate should consider the amount of energy injected in the ICM as the shock wave passes through it, and despite the number of assumptions and approximations, we suggest that the relic indicates the position of the merger center as it was ~ 0.4 Gy ago. The time that the shock wave has taken to get the present relic position is the time that the sub cluster has taken to get the current X-ray center position.

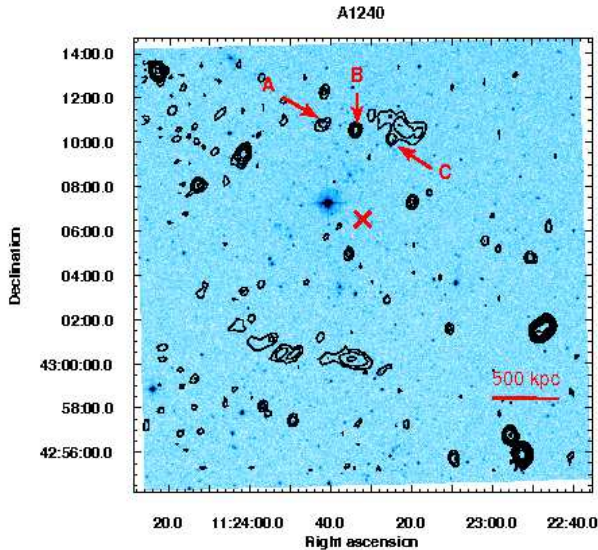


Fig. 6. Abell 1240. Colors: Optical emission from DPOSSII (red band); Contours: radio emission at 1.4 GHz (HR image). Contours start at $\pm 3\sigma$ and are then spaced by 2. Red cross signs the X-ray center, labels refer to the discrete sources embedded in A1240-1.

4. The Cluster Abell 1240

Little is known in the literature about this cluster. It is a rich cluster classified as Bautz-Morgan type III. In Tab. 5 general data about this cluster are reported.

Kempner & Sarazin (2001) have revealed the presence of two roughly symmetric relics from the Westerbork Northern Sky Survey (WENSS). From WENSS images relics are visible at 2 and 2.5σ level. Our VLA observation confirm the presence of two weak radio emitting regions in the cluster's outskirts. The radio image of the cluster is shown in Fig. 6 (contours) overlaid into optical emission (from the DPOSSII, red band). The Northern relic (A1240-1) is located at $\sim 270''$ from the cluster X-ray center. This distance corresponds to ~ 700 kpc at the cluster's redshift. This relic is mainly elongated in the E-W direction, and its radio brightness decreases going from the western to the eastern part of the relic (see Fig. 7). At 325 MHz only the eastern brightest part is visible. This is likely due to the higher noise in the 325 MHz image. In fact from the mean brightness of the weaker part of the relic, we estimated that it should have a spectral index >3 to be detected at 325 MHz. Three radio sources are embedded in the relic emission, they are labeled with A B and C in Fig. 6. The sources A and B are not detected in the 325 MHz observations. This is consistent with spectral index values <1 , as commonly found in radiogalaxies. A weak emission at 1.4 GHz links the A radio source at the relic (see Fig. 7).

The southern relic (A1240-2) is located at $\sim 400''$ (1.1 Mpc) from the cluster X ray center. At 1.4 GHz it is elongated in the E-W direction extending $\sim 480''$. No discrete sources have been found embedded in the relic emission. Also in this case at 325 MHz the relic's extension is reduced to $\sim 350''$ along the main axis, and only the brightest regions are visible at 325 MHz.

The relic's physical parameters are reported in Tab. 7. The quantity are computed excluding the region where discrete sources (A,B and C) are present.

4.1. Spectral index analysis

We report in Fig.7 the spectral index map and the spectral index map error for the relics of Abell 1240. They have been obtained considering only those pixels that have a brightness $>2\sigma$ at both frequencies.

Fig. 7 shows that the spectral index image is patchy. The spectral index image rms, σ_{spix} , is ~ 0.3 and 0.4 for A1240-1 and A1240-2 respectively, while the mean of the spectral index error image, $\langle Spix \text{ Noise} \rangle$ is ~ 0.2 for both of the relics. We can then conclude that features in A1240-2 are statistically significant, while given the small difference between σ_{spix} and $\langle Spix \text{ Noise} \rangle$ in A1240-1, we cannot exclude that local features are a noise artifact in this case. In the relic A1240-2 a gradient is visible along the main axis of the relic, as has been found in Abell 2256 by Clarke & Ensslin (2006).

In Fig. 8 the radial spectral index trend is shown for A1240-1 and A1240-2 respectively. They have been obtained as described in Sec. 3.1. Spherical shells are centered close to the X-ray cluster center and they are parallel to the main axis of both relics.

Despite the small extension of the relics at 325 MHz, it is still possible to derive some important results on the spectral index radial trends in these relics: in the relic A1240-1 the spectral index is steeper in the inner part of the relic and flatter in the outer part, as found in A2345-2 and predicted by "outgoing merger shock" models if relics are seen edge-on (Roettiger et al. 1999;

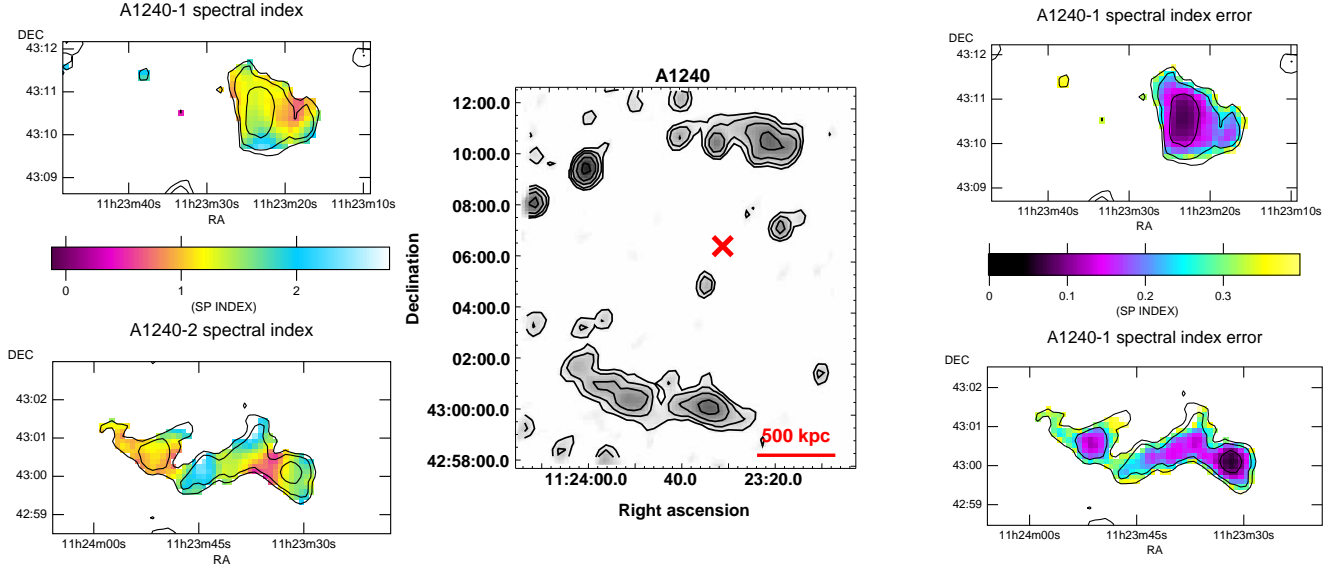


Fig. 7. Center: the cluster Abell 1240 radio emission at 1.4 GHz. The beam is $42'' \times 33''$. Contours start at 3σ (0.13 mJy/beam) and are then spaced by a factor 2. The cross marks the cluster X-ray center. Left: colors represent the spectral index of the relic A1240-1 (top) and A1240-2 (bottom) superimposed over the radio emission at 325 MHz (contours) The beam is $42'' \times 33''$, first contours are 2σ (2 mJy/beam), 3σ and are then spaced by a factor 2. Right: Spectral index error image (colors) superimposed onto the emission at 325 MHz (contours are as above).

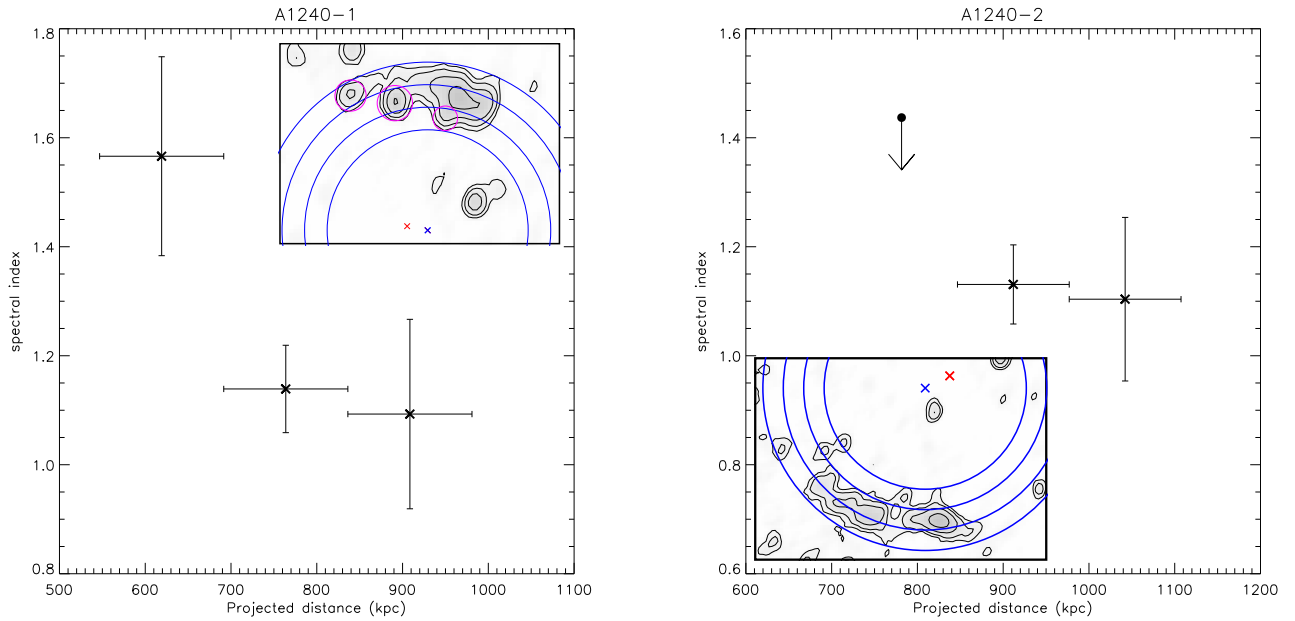


Fig. 8. Spectral index radial trend of A1240-1 (left) and A1240-2 (right), computed in shells of $\sim 50''$ in width. It has been computed excluding the contribution of the discrete sources. Crosses refer to spectral index values computed in shells where the mean brightness is $> 3\sigma$ at both 325 MHz and 1.4 GHz. Arrows are 3σ upper limits on the spectral index mean value (see text). In the inset: displacement of the shells over which the mean spectral index has been computed. Circles refer to the discrete sources embedded in the relic emission. The red cross refers to the cluster X-ray center, the blue cross is the center of the spherical shells.

Bagchi et al. 2006). The same trend is consistent with the spectral index profile derived in A1240-2, although a firm conclusion cannot be derived from these data. We note in fact that errors and upper limit in the inner shell cannot exclude a constant spectral index or even an opposite trend.

4.2. Radio-X-ray comparison

We retrieved from the ROSAT data archive X-ray observations in the energy band 0.5 – 2 keV. The cluster is $\sim 28'$ offset from the center of the ROSAT pointing. Observations have been performed with the ROSAT PSPC detector for a total exposure time of ~ 12 ksec. After background subtraction the event file has

Table 7. Abell 1240

Source name	Proj. dist kpc	LLS kpc	F_{20cm} mJy	F_{90cm} mJy	$B_{eq} - B'_{eq}$ μG	$\langle \alpha \rangle$
Abell 1240-1	$270''=700$	$240''=650$	6.0 ± 0.2	21.0 ± 0.8	1.0-2.4	1.2 ± 0.1
Abell 1240-2	$400''=1100$	$460''=1250$	10.1 ± 0.4	28.5 ± 1.1	1.0-2.5	1.3 ± 0.2

Col. 1: Source name; Col. 2: projected distance from the X-ray centroid; Col. 3: Largest linear scale measured on the 20 cm images.

Col. 4 and 5: Flux density at 20 and 90 cm; Col. 6: equipartition magnetic field computed at fixed frequency - fixed energy (see Sec. 4.3)

Col. 7: mean spectral index in region where both 20 cm and 90cm surface brightness is $> 3\sigma$.

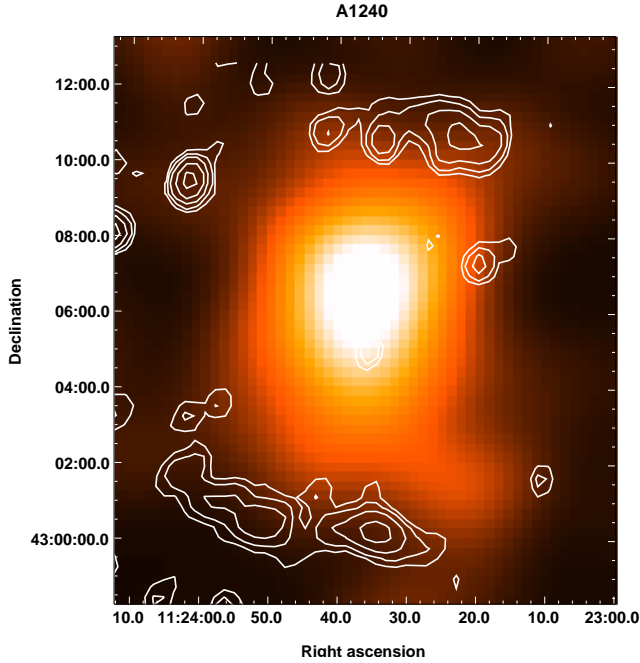


Fig. 9. Colors: Abell 1240 X-ray emission in the energy band 0.5-2 keV from ROSAT PSPC observations. The image has been smoothed with a Gaussian of $\sigma \sim 60''$; contours represent the radio image of the cluster at 1.4 GHz. The beam is $42'' \times 33''$. First contour is 0.13 mJy/beam, further contours are then spaced by a factor 2.

been divided by the exposure map. We smoothed the resulting image with a Gaussian of $\sigma = 60''$. The resulting image is shown in Fig. 9.

In Fig. 9 the X-ray emission of the cluster is superimposed onto radio contours. The X-ray emission of this cluster is elongated in the S-N direction and shows a double X-ray morphology. As already stated by Kempner & Sarazin (2001) this morphology is consistent with a slightly asymmetric merger.

Relics are located at the edge of the X-ray emission. Their emission shows the characteristic elongated shape, and their main axis is perpendicular to the main axis of the X-ray emission, as found in double relics of Abell 3367 and Abell 3376.

4.3. Equipartition magnetic field

Under the same assumptions explained in Sec. 3.4, we calculated the equipartition magnetic field for the relics A1240-1 and A1240-2. Values obtained are reported in Tab. 7. We note that these values have been computed considering the brightness of those pixels for which we have well constrained information about the spectral index value, i. e. those regions whose emis-

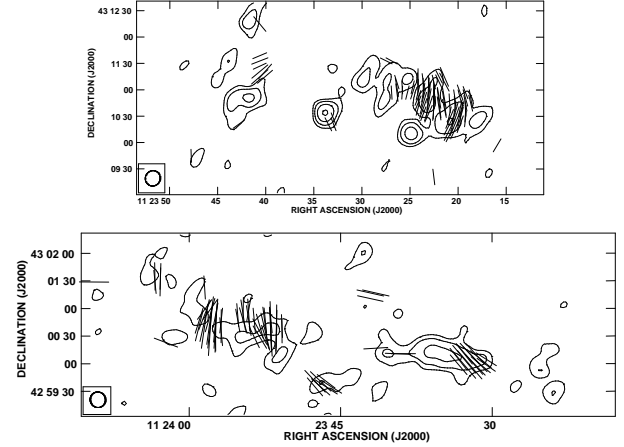


Fig. 10. Top panel: A1240-1 radio emission at 1.4 GHz, lines represent the E vectors. The line direction indicates the E vector direction and the line length is proportional to the polarized flux intensity. $1''$ corresponds to $3\mu\text{Jy}/\text{beam}$. The beam is $18'' \times 18''$. Contours start at 0.12 mJy/beam and are then spaced by a factor 2. Bottom panel: A1240-2 radio emission at 1.4 GHz. The line direction indicates the E vector direction and the line length is proportional to the polarized flux intensity. $1''$ corresponds to $2\mu\text{Jy}/\text{beam}$. Contours are as above.

sion is detected at both frequencies. Since the emission at 325 MHz is only detected in a small region of the relics, while at 1.4 GHz relics are more extended, the equipartition estimates refer to the same small regions, and different estimates could be representative of the wider relic emission detected at 1.4 GHz.

We derived the minimum non thermal energy density in the relic sources from B'_{eq} obtaining $U_{min} \sim 5.5 \cdot 10^{-13} \text{erg}/\text{cm}^{-3}$ for A1240-1 and A1240-2. The corresponding minimum non-thermal pressure in then ~ 3.4 and $\sim 3.5 \cdot 10^{-13} \text{erg}/\text{cm}^{-3}$. The consistency between magnetic field equipartition values and magnetic field lower limits derived by X-ray emission in other few clusters (see discussion in Sec. 3.3) indicates that equipartition magnetic field can be used as a reasonable approximation of the magnetic field in relics.

4.4. Polarization analysis

We obtained the polarized intensity images for the relics as described in Sec. 3.4. In Tab. 4 the parameters relative to the polarization images of the relics A1240-1 and A1240-2 are reported. In Fig. 10 the polarized emission of the two relics is shown. Observations performed with C array cannot reveal the weak extended emission, and thus only the most compact and bright regions are visible in this image. In these regions the magnetic field is mainly aligned along the relic main axis in both of the relics. This is consistent with what has been observed in the

relics of Abell 2345 and with what is expected from the models that explain the origin of these sources (e. g. Ensslin et al. 1998; Roettiger et al. 1999). The mean fractional polarization of A1240-1 is 26%, reaching values up to 70%. In the relic A1240-2 the mean fractional polarization is 29%, reaching values up to 70%. From Eq. 1 we derive that $B_r^2/B_o^2 \sim 1.4$ and 1.2 respectively. Because of possible beam depolarization, internal depolarization and ICM depolarization, we conclude that $B_r^2/B_o^2 < 1.4$ and < 1.2 . This means that the magnetic energy density in the random and ordered component is similar.

4.5. Results on Abell 1240

Our observations confirm the presence of two relics in Abell 1240 with as steep spectral index values as ~ 1.2 and ~ 1.3 . The spectral index trends derived for these relics indicate a radial flattening toward the cluster outskirts. This is the trend predicted by “outgoing merger shock” models.

The double relics radio morphology and location are similar to the double relics found in Abell 3667 and Abell 3376.

The polarization level is high in both of the relics, although we have to consider that our polarization observations lack the weak extended regions, that are probably less polarized. The magnetic field estimate achieved under the minimum total energy assumption reveals magnetic field of the order of μG at the cluster periphery in the relic regions, ordered on Mpc scale, indicating a magnetic field amplification and ordering.

5. Discussion

We confirm the presence of double relics in the cluster Abell 1240. Their symmetry and properties strongly suggest a common origin of A1240-1 and A1240-2.

In the cluster Abell 2345 we confirm the existence of two relics. However, while A2345-2 is a classic extended peripheral relic source similar to 1253+275, in the Coma cluster (see Giovannini et al. 1991 and references therein), A2345-1 shows a more complex structure. We suggest that its properties could be due to its peculiar position in between the cluster Abell 2345 and the possibly merging group X1, and thus affected by a more recent merger.

Several models have been proposed to explain the origin of radio relics. They can be divided into 2 classes:

1. Diffusive Shock Acceleration by Fermi-I process (Ensslin et al. 1998; Roettiger et al. 1999; Hoeft & Brüggen 2007).
2. Re-acceleration of emitting particles due to adiabatic compression of fossil radio plasma (Ensslin & Gopal-Krishna 2001).

In both of these models the presence of a shock within the gas is required. The second one also requires the presence of a nearby radio source to provide the fossil radio plasma which can be re-energized by the shock wave. Simulations of cluster mergers show indeed that the merging of two sub-clusters leads to the formation of shocks in the cluster outskirts (Ryu et al. 2003).

In favor of the second scenario there is the observational evidence that relics resemble individual objects and do not trace the entire shock front (Hoeft et al. 2004). Moreover, when a radio ghost is passed by a shock wave with typical velocity of 10^3 km/s, it is adiabatically compressed because of the higher value of the sound speed in the radio ghost (Ensslin & Brüggen 2002). We have to remind, however, that the equation of state of the radio emitting plasma is still poorly known, and that if the radio

plasma has a high mass load due to undetectable cool gas, it should get shocked (Ensslin & Gopal Krishna 2001).

The presence of double relics itself favors the first scenario, because of the low probability to find two symmetric regions with fossil radio plasma.

Several independent cosmological simulations have identified two main categories of cosmological shocks:

- (i) “accretion shocks” resulting from accretion of cold gas onto already formed structure, characterized by high Mach numbers;
- (ii) “merging” or “internal” shocks due to merging of substructures such as galaxy clusters or groups, with moderate Mach numbers: $2 \leq M \leq 4$ (see review by Bykov et al. 2008 and references therein).

5.1. Relics from merging shocks

The presence of double relics is particularly interesting in this scenario since the shape, morphology and properties of these extended structures strongly suggest the presence of shock waves propagating from the cluster center to the peripheral regions. Because of the short radiative lifetime of relativistic electrons, radio emission is produced close to the location of the shock waves. These models predict that the magnetic field is aligned with the shock front and that the radio spectrum is flatter at the shock edge, where the radio brightness is expected to decline sharply.

The shock compression ratio can be estimated from the radio spectral index α (assuming an equilibrium electron population accelerated and cooled at the same time, and assuming a polytropic index $5/3$, see Drury 1983), as

$$R = \frac{\alpha + 1}{\alpha - 0.5}. \quad (2)$$

The pressure and temperature jumps across the shock can be estimated from the theory of shocks (Landau & Lifschitz 1966) as

$$\frac{P_2}{P_1} = \frac{4R - 1}{4 - R} = \frac{\alpha + 1.5}{\alpha - 1}; \quad \frac{T_2}{T_1} = \frac{P_2}{RP_1} \quad (3)$$

here and after the index 2 refers to down stream regions and 1 to up-stream regions i.e. regions inside and outside the cluster shock front. These parameters are reported in Tab. 8. The Mach number of the shock can be estimated from the radio spectral index under some assumptions: if the emitting particles are linearly accelerated by shock, the spectral index of the particle energy spectrum p ($= 2\alpha + 1$) is related to the Mach number M of the shock through:

$$p = 2 \frac{M^2 + 1}{M^2 - 1} + 1 \quad (4)$$

including the effect of particle aging (continuous injection and Inverse Compton energy losses, see e.g. Sarazin 1999). Mach number values we obtained are reported in Tab. 8. These values are lower than Mach number expected for accretion shocks (e. g. Bykov et al. 2008), and are instead consistent with those expected for weaker shocks due to merging of structures.

The spectral index trend clearly detected in A2345-2 and in both relics of Abell 1240 agrees with the predictions of this scenario. If relics are seen edge-on, the flattest region, in the outer part of the relics, would corresponds to the current shock location, indicating shock waves moving outward from the cluster center. As discussed in Sec. 3.5, A2345-1 shows a more complex radio emission. It could be affected by a more recent merger with

Table 8. Predictions from the shock acceleration model

Relic	α	M	R	P_2/P_1	T_2/T_1	$(B_2/B_1)_{isoP}$
Abell 2345-1	1.5±0.1	2.8±0.1	2.5±0.2	6±1	2.4±0.4	2.4±0.2
Abell 2345-2	1.3±0.1	2.2±0.1	2.9±0.2	9±3	3±1	3.0±0.5
Abell 1240-1	1.2±0.1	3.3±0.2	3.1±0.3	14±6	4±2	3.7±0.8
Abell 1240-2	1.3±0.2	2.8±0.3	2.9±0.4	9±3	3±2	3.0±0.5

Col. 1: Source name; Col 2: spectral index value; Col. 3: Mach number; Col 4: Shock compression ratio estimated from the radio spectral index; Col. 5, 6: Pressure and temperature jump across the shock; Col. 7: Magnetic field strength in the pre and post shock regions required to support the relic against the thermal pressure

the X1 group. It could trace a merger shock moving inward to the cluster center as a result of the Abell 2345 - X1 group interaction.

5.1.1. Magnetic field and merging shocks

The study of the magnetic field associated with the relics offers further opportunities to investigate the connection between relics and merger shock waves. First of all the presence of relics itself indicates the existence of significant magnetic field at the cluster periphery on the Mpc scale. Furthermore, the detected level of polarization shows that the magnetic field in these regions is rather ordered.

The effect of passage of a shock wave in the ICM could be twofold: (i) order and compress a magnetic field that was randomly oriented before the shock passage or (ii) compress a magnetic field that was already ordered on the relic scale before the shock passage. This depends on the turbulence development at the cluster periphery, that could either give rise to a random field in the cluster outskirts (case i) or not (case ii). Little is known about this point from observational point of view. Observational evidence from the gas pressure map of the Coma cluster (Schuecker et al. 2004) indicates the relevance of chaotic motions within the ICM. Cosmological numerical simulations (e.g. Bryan & Norman 1998; Sunyaev, Bryan & Norman 2003) suggest that the level of ICM turbulence is larger at increasing radial distances from the cluster center. If the simple Kolmogorov's picture of incompressible fluid turbulence is assumed, this implies a more developed turbulence in the outermost region (since the decay time is L/σ , where L is the typical scale where the bulk of turbulence is injected, and σ is the rms velocity of turbulence). Recently Ryu et al. (2008) argued that turbulence is likely well developed in clusters and filaments, and not in more rarefied regions such as sheets and voids. On the other hand Dolag et al. (2005) suggested that the bulk of turbulence is injected in the core of galaxy clusters, thus implying a more developed turbulence in the innermost regions, compared to the outermost ones. The main limitation of cosmological simulations is the lack of resolutions in low density environments, that makes it difficult to discriminate if the turbulent cascade is developed in these regions. Moreover, details of the conversion process of largescale velocity fields into MHD modes is still poorly understood. Thus, from the theoretical point of view the overall picture seems still uncertain.

In the case that the magnetic field in the cluster outskirts is randomly oriented before the shock passage (i. e. the turbulence is developed in the cluster outskirts) and that it has been amplified and ordered, by the passage of the shock wave (case i above), the observed ratio B_r/B_o derived by polarization analysis (Sec. 3.4 and 4.3) could be used to estimate the magnetic field amplification due to the passage of the shock.

Following Ensslin et al. (1998), if the relic is seen at some angle $\delta > 0$ between the line of sight and the normal of the shock front, the projected magnetic field should appear perpendicular to the line connecting the cluster center and the relic. This is indeed what polarization data presented here show. The magnetic field amplification, the observed integral polarization and the preferential direction of the field revealed by the E vectors orientation could be derived, provided that δ and R, the shock compression factor, are known. Present data do not allow to infer the angle δ . Future X-ray and optical observations could reconstruct the merging geometry for these two clusters, as done, e.g. in Abell 521 by Ferrari et al. (2003, 2006). Despite this, if relics are supported by magnetic pressure only, the upstream and downstream fields are related by $(B_2^2/B_1^2)_{isoP} = P_2/P_1$ ("strong field" case in Ensslin et al. 1998). This ratio can be compared to the ratio derived by the polarization properties of the relics, under the assumption that B_2 corresponds to the ordered component of the field and B_1 to the random one. In Tab. 8 the $(B_2/B_1)_{isoP}$ ratio is reported for the relics in Abell 2345 and Abell 1240. These values are comparable to the observed ratio B_r/B_o derived by polarization analysis (Sec. 3.4 and 4.3).

Another indication of the magnetic field amplification in the relics may be obtained by comparing the magnetic field in the relic with the cluster magnetic field intensity expected at the relic location. Relics are located at 700-1100 kpc from the cluster center in Abell 2345 and Abell 1240. At these distances the cluster magnetic field strength is expected to be of the order of $\sim 10^{-1} \mu\text{G}$ (see e. g. Dolag et al. 2008; Ferrari et al. 2008 and references therein). Equipartition magnetic field values are of the order of μG (see Sec. 3.3 and 4.3), thus about 10 times higher. Despite the number of uncertainties and assumptions related with the equipartition estimate, this is consistent with the ratio $(B_2^2/B_1^2)_{isoP}$ and B_r/B_o .

Even if no firm conclusion can be obtained by this analysis, we can conclude at least that the drawn picture has no inconsistencies with the presented observations.

5.2. Relics from Adiabatic compression

Another model to explain the origin of cluster radio relics has been proposed by Ensslin & Gopal-Krishna (2001). This idea has been investigated with the help of 3-dimensional Magneto Hydro Dynamical simulations by Ensslin & Brüggen (2002) and in a more realistic cosmological environment by Hoeft et al. (2004). In this scenario cluster radio relics would originate by the compression of fossil radio plasma by shock wave occurring in the process of large scale structure formation. The expected high sound velocity of that still relativistic plasma should forbid the shock to penetrate into the radio plasma, so that shock acceleration is not expected in this model. The plasma gains energy adiabatically from the compression and the magnetic field itself is amplified by such compression. If the electron plasma is not

older than 2 Gyr in the outskirts of a cluster, they can emit radio wave again. Simulations performed by Ensslin & Brüggen (2002) show that the radio morphology of the resulting radio relic in the early stage after the shock passage is sheet-like. Then the formation of a torus is expected when the post shock gas starts to expand into the volume occupied by the radio plasma. Thus it is expected in this scenario that some correlation should exist between the morphology of the radio relic and its spectral index, that traces the time passed after the shock wave has compressed and re-energized the emitting particles. A2345-1 shows indeed a torus-like radio structure and a spectral index higher than A2345-2, A1240-1 and A1240-2, that exhibit a sheet-like structure. The simulations performed by Ensslin & Brüggen (2002) indicate that the compression of the radio plasma by the shock can be estimated from a cluster radio relic with a toroidal shape. Assuming the idealized case of a initially spherical and finally toroidal radio cocoon, the compression factor is given by:

$$R' = \frac{2r_{max}^2}{3\pi r_{min}^2} \quad (5)$$

where r_{max} and r_{min} refer to the outer and inner radius of the torus. In the case of A2345-1 we assume that the observed torus like structure can be described by taking $r_{max} \sim$ the LLS of the relic and r_{min} the thickness of the filament in the N-E part of the relic, as suggested by the same authors in the case of non perfect toroidal filamentary relics. With $r_{max} \sim 1$ Mpc, $r_{min} \sim 200$ kpc it results $R' \sim 5$. This is higher than the value of the maximum compression ratio for mono-atomic gas (that is 4); this would indicate that the radio plasma has a different equation of state. However no conclusion can be drawn since Eq. 5 is based on too simplistic assumptions, in particular a spherical model for the compressed relic.

6. Conclusions

We have presented 1.4 GHz and 325 MHz observations of Abell 2345 and Abell 1240. The presence of double relics in these cluster had been inferred by Giovannini et al. (1999) for Abell 2345 and by Kempner & Sarazin (2001) for Abell 1240 from NVSS and WENSS. We confirm the presence of two relics in each of these clusters. By combining 1.4 GHz and 325 MHz observations we obtained the spectral index image of the diffuse radio emission. The study of the polarized emission at 1.4 GHz has been presented as well. The analysis of both the spectral index distribution and the polarization properties of relics allows to test several independent predictions of the relic formation models.

We report the summary of the results from the presented analysis:

1. **A2345:** two relics have been detected in the cluster outskirts at both 1.4 GHz and 325 MHz. They are not perfectly symmetrical with respect to the cluster center; the normals to the relic main axis form an angle of $\sim 150^\circ$. A2345-2 is a classical peripheral relic and A2345-1 is a peculiar relic with a torus-like structure possibly related to a merging region.
2. **A1240:** relics are fainter than relics in A2345. Their extended emission is detected at 1.4 GHz while only their brightest part are detected at 325 MHz. They are symmetrical with respect to the cluster center and the angle between

their normals is $\sim 180^\circ$ as found in the other known double relics: Abell 3667, Abell 3376 and RXCJ1314.4-2515.

3. Relics are located at the edge of the X-ray emission of Abell 2345 and Abell 1240. The X-ray emission of Abell 2345 shows multiple substructures that could be galaxy groups interacting with A2345. Peculiar features of A2345-1 could arise from this multiple interaction, but only detailed X-ray and optical analysis could shed light on this point.
4. Relics in Abell 1240 are located perpendicular to the cluster main axis revealed by X-ray observations. The double X-ray morphology of the cluster is typical of merging clusters.
5. The average spectral indexes are steep. We found 1.5 ± 0.1 and 1.3 ± 0.1 for A2345-1 and A2345-2 and 1.2 ± 0.1 , 1.3 ± 0.2 for A1240-1 and A1240-2.
6. The spectral index distribution in the relics is rather irregular and patchy, although this, a clear radial trend is present in the relics of these two clusters. A2345-2 spectral index ranges from ~ 1.5 in the region closer to the cluster center to ~ 1.1 in the outer rim. This trend is consistent with shock models predictions. The same trend is observed in both of Abell 1240 relics. A1240-1 spectral index ranges from ~ 1.1 to ~ 1.6 going from the outer to the inner rim, A1240-2 spectral index is also consistent with a similar trend (going from $\alpha < 1.5$ in the inner rim to $\alpha \sim 1.1$ in the outer one). An opposite trend is instead detected in A2345-1. Spectral index values are lower in the inner rim (~ 1.3) and increase toward the outer part of the relic reaching values ~ 1.7 . This trend could be due to its peculiar position between two merging clumps.
7. The magnetic field, as revealed by polarized emission is mainly aligned with the relic main axis. In Abell 2345 the polarized emission reveals the arc-like structure morphology of the relic A2345-2. Under equipartition conditions, values of $\sim 2.2 - 2.9 \mu\text{G}$ are derived. The field has been likely amplified, consistently with shock models predictions.

These results have been discussed in the framework of relic formation models. The Mach numbers derived from the value of radio spectral index disfavour the ‘‘accretion shock’’ scenario, since they are too small. Outgoing merger shock waves, proposed to explain double relic emission in Abell 3667 and A3376, could also work in Abell 1240 and Abell 2345. For the latter cluster we suggest that the peculiar emission of A2345-1 could be explained by a shock wave moving inward, due to the interaction of the main cluster with the X1 group.

The toroidal shape of A2345-1 could be produced by adiabatic compression, however the available data and models do not allow a conclusive comparison.

Acknowledgements. The authors grateful to Franco Vazza, Marica Branchesi and Elisabetta Liuzzo for helpful discussions and to Klaus Dolag for elucidating discussion on cluster magnetic fields. The authors thank the anonymous referee for useful suggestions and comments. NRAO is a facility of the National Science Foundation, operated under cooperative agreement by Associated Universities, Inc. This work was partly supported by the Italian Space Agency (ASI), contract I/088/06/0, by the Italian Ministry for University and Research (MIUR) and by the Italian National Institute for Astrophysics (INAF). This research has made use of the NASA/IPAC Extragalactic Data Base (NED) which is operated by the JPL, California Institute of Technology, under contract with the National Aeronautics and Space Administration.

References

- Andernach H., Feretti L., & Giovannini G., 1984, *A&A*, 133, 252
- Baars, Jacob W.M. & Martin, Robert M. 1990, *LIACo*, 29, 293
- Bagchi, J., Durret, F., Lima Neto, G.B., & Paul, S. 2006, *Science*, 314, 791
- Beck, R. & Krause, M. 2005, *AN*, 326, 414
- Böhringer, H. et al. 2004, *A&A*, 425, 367
- Bykov, A.M., Dolag, K., & Durret, F. 2008, *SSRv.*, 134, 119
- Brunetti, G., Setti, G., & Comastri, A. 1997, *A&A*, 325, 898
- Bryan G.L. & Norman M.L. 1998, *ApJ*, 495, 80
- Burn, B.J. 1966, *MNRAS* 133 67
- Chen, C.M.H., Harris, D.E., Harrison, F.A., & Mao, P.H. 2008, *MNRAS*, 383, 1259
- Clarke, T.E., & Ensslin, T.A. 2006, *AJ*, 131, 2900
- Cypriano, E.S., Sodré, L.J., Kneib, J.P., Campusano, L.E. 2004, *ApJ* 613 95
- Dahle, H., Kaiser, N., Irgens, R.J., Lilje, P.B., & Maddox, S.J. 2002 *ApJ* 139 313
- David, L.P., Forman, W., & Jones, C. 1999, *ApJ*, 519, 533
- Dolag, K., Bykov, A.M., & Diaferio, A. 2008, *SSRv*, 134, 311
- Dolag, K., Schindler, S., Govoni, F., & Feretti, L. 2001, *A&A*, 378, 777
- Dolag K., Vazza F., Brunetti G., & Tormen G. 2005, *MNRAS*, 364, 753
- Drury, R.O. 1983, *Reports on Progress in Physics*, 46, 973
- Ensslin, T.A., Biermann, P.L., Klein, U., & Kohle, S. 1998, *A&A*, 332, 395
- Ensslin, T.A., & Brüggén, M. 2002, *MNRAS*, 331, 1011
- Ensslin, T.A., & Gopal-Krishna 2001, *A&A*, 366, 26
- Feretti, L., & Neumann, D.M. 2006, *A&A*, 450, L21
- Feretti, L., Schuecker, P., Böhringer, H., Govoni, F., & Giovannini, G. 2005, *A&A* 444 157
- Ferrari, C., 2003, “Multi-wavelength analysis of merging galaxy clusters”, PhD Thesis, available electronically at <http://tel.archives-ouvertes.fr/docs/00/04/85/55/PDF/tel-00010416.pdf>
- Ferrari, C., Maurogordato, S., Cappi, A., & Benoist, C., 2003, *A&A*, 399, 813
- Ferrari, C., Arnaud, M., Ettori, S., Maurogordato, S., & Rho, J., 2006, *A&A*, 446, 417
- Ferrari, C., Govoni, F., Schindler, S., Bykov, A.M., & Rephaeli, Y. 2008, *SSRv*, 134, 93
- Giacintucci, S., Venturi, T., Macario, G., et al. 2008, *A&A* in press, 2008arXiv0803.4127G
- Giovannini, G., Feretti, L., & Stanghellini, C. 1991, *A&A*, 252, 528
- Giovannini, G., & Feretti, L. 2004, *Journal of the Korean Astronomical Society*, Proceedings of the 3rd Korean Astrophysics Workshop “Cosmic Rays and Magnetic Fields in Large Scale Structure”, Pusan, Korea, August 2004, eds. H. Kang & D. Ryu, 37, 1
- Giovannini, G., Tordi, M., & Feretti, L. 1999, *New Astron.*, 4, 141
- Govoni, F., & Feretti, L. 2004, *IJMPD*, 13, 1549
- Henriksen, M., & Mukshotzky, R. 2001, *ApJ*, 553, 84.
- Hoefl, M., Brüggén, M., & Yepes, G. 2004, *MNRAS*, 347, 389
- Hoefl, M., & Brüggén, M. 2007, *MNRAS*, 375, 77
- Johnston-Hollitt, M., Clay, R.W., Ekers, R.D., Wieringa, M.H., & Hunstead, R. W. 2002 *IAUS* 199, 157
- Kempner, J.C., & Sarazin, C.L. 2001, *ApJ*, 548, 639
- Kempner, J.C., et al. 2004, in “The riddle of cooling flows in galaxies and clusters of galaxies”, T. Reiprich, J. Kempner & N. Soker (eds.), published electronically at <http://www.astro.virginia.edu/coolingflow/>
- Landau L.D. & Lifshitz, E.M. 1966, *Fluid Mechanics*, (Pergamon Press Ltd.)
- Orrú, E., Murgia, M., Feretti, L., et al. 2007, *A&A*, 467, 943
- Owen, F.N., Brogan, C.L., & Clarke T.E. 2004, published electronically at <http://www.vla.nrao.edu/astro/giudes/p-band/p-reduction/>
- Pacholczyk, A.G. 1970, *Radio astrophysics*, (Freeman Eds.)
- Pizzo, R.F., de Bruyn, A.G., Feretti, L., & Govoni, F. 2008, *A&A*, 481L 91
- Roettiger, K., Burns, J.O., & Stone, J.M. 1999, *ApJ*, 518, 603
- Röttgering, H.J.A., Wieringa, M.H., Hunstead, R.W., & Ekers, R.D. 1997, *MNRAS*, 290, 577
- Ryu, D., Kang, H., Hallman, E., & Jones, T. W. 2003, *ApJ*, 593, 599
- Ryu D., Kang H., Cho J., & Das S. 2008, *Science*, 320, 909
- Sarazin, C.L. 1988, *X-ray emission from clusters of galaxies*, (Cambridge University Press)
- Sarazin, C.L. 1999, *ApJ*, 520, 529
- Schuecker P., Finoguenov A., Miniati F., Böhringer H., & Briel U.G. 2004, *ApJ*, 426, 387
- Solovyeva, L., Anokhin, S., Feretti, L., et al. 2008, *A&A* 484 621
- Sunyaev, R. A., Norman, M. L., & Bryan, G. L. 2003, *AstL* 29, 783
- Venturi, T., Giacintucci, S., Brunetti, G., et al. 2007, *A&A* 463 937